


Two-Dimensional Measurement of Airborne Ultrasound Field Using Thermal Images

Ryoya Onishi¹,* Takaaki Kamigaki¹, Shun Suzuki¹, Tao Morisaki¹, Masahiro Fujiwara¹, Yasutoshi Makino¹, and Hiroyuki Shinoda¹

Graduate School of Frontier Sciences, The University of Tokyo, Kashiwa-shi, Chiba 277-8561, Japan

 (Received 22 April 2022; revised 12 August 2022; accepted 15 September 2022; published 19 October 2022)

Recently, the applications of airborne ultrasound technology have garnered considerable attention; however, high-speed ultrasound field measurements in air have not been well researched. This study demonstrates that thermal responses to high-intensity airborne ultrasound can be used to visualize airborne ultrasound fields. Thermal images on a mesh screen enable the rapid quantitative measurement of two-dimensional ultrasound fields. Additionally, based on the temperature distribution on a surface that reflects ultrasound waves, it is possible to determine the ultrasound focus position with a resolution much finer than the wavelength. The results demonstrate that thermography observations based on ultrasound-temperature conversion, which are conventionally time-consuming or difficult to perform, can be used to visualize acoustic fields within 0.5 s. These findings will advance engineering applications that use strong airborne ultrasound, such as midair haptics and acoustic levitation, and provide scientific and technical applications for detecting surface properties and composition, including those of cells and fragile materials.

DOI: [10.1103/PhysRevApplied.18.044047](https://doi.org/10.1103/PhysRevApplied.18.044047)

I. INTRODUCTION

Applications that utilize the high-intensity airborne ultrasound waves generated by ultrasound phased arrays, such as acoustic levitation [1–3], midair haptics [4,5], and airflow control [6], are receiving increasing attention. Measurement of the ultrasound field is essential in such applications, and microphones and optical methods have been used for this purpose.

However, a high-speed measurement method for airborne ultrasound fields has not been well established. The current practical method is mechanical scanning using a microphone. Another technique is Schlieren imaging [7,8]; however, because the obtained physical quantities are integrated into the optical path, quantitative ultrasound measurement requires measurement from various angles, which takes time.

The time-consuming nature of these measurements is a critical limitation for some applications. In midair haptics, which is an important application of high-intensity airborne ultrasound, the inability to check the conditions

of ultrasound irradiation in real time is detrimental. When ultrasound is irradiated to the fingertip, the focus position may shift by several millimeters depending on the air temperature. Furthermore, focusing is impaired by diffraction from surrounding objects, significantly affecting the tactile sensation.

This paper reports the measurement of an airborne ultrasound field using temperature data. By inserting a mesh screen into the airborne ultrasound field and measuring the surface temperature using a thermography camera, the two-dimensional sound pressure distribution can be visualized within 0.5 s. Further, by scanning the mesh screen, the three-dimensional sound pressure distribution can be measured at high speed. Furthermore, we observe the temperature distribution corresponding to the ultrasound field on a skin surface that reflects 99.95% of 40-kHz airborne ultrasound [9].

The measurement approach of visualizing ultrasound by absorbing and converting it into heat was proposed in the 1970s [10]. This method has been continuously studied since then for the measurement of ultrasound fields in water and *in vivo* [11–14]. The measurement mechanism described in this paper is different from those in water and tissue. As the ultrasound attenuation in the air is more significant and the thermal conductivity is smaller than that in water or in tissue, the air itself develops a three-dimensional temperature rise distribution corresponding to the sound pressure distribution. This situation enables a

* onishi@hapis.k.u-tokyo.ac.jp

Published by the American Physical Society under the terms of the [Creative Commons Attribution 4.0 International](https://creativecommons.org/licenses/by/4.0/) license. Further distribution of this work must maintain attribution to the author(s) and the published article's title, journal citation, and DOI.

sufficient temperature rise even on the surface of an object that completely reflects ultrasound, from which sound field information can be obtained.

The proposed method contributes to the development of conventional airborne ultrasound applications. First, it enables the practical reproducibility verification of sound fields in general laboratory experiments. A sound field can be corrected through rapid repeating measurements and output adjustments. In addition, as experiments can be conducted while directly observing the pressure distribution applied to the surface, levitation of heavier objects and precise tactile presentation can be expected. Furthermore, this article presents exploratory research on the effects of using airborne ultrasound on the skin, as well as scientific and technical tools for elucidating the surface properties of fragile materials such as cells.

II. PROPOSED METHODS

In the airborne ultrasound field, the temperature of the air, which is the medium, rises where the sound pressure is high. It is possible to estimate the two-dimensional sound pressure distribution by measuring the two-dimensional temperature distribution of the air. We estimate the temperature distribution in this study by capturing a thermal image of the surface of an object (nylon mesh) having a small heat capacity inserted into the ultrasound field.

According to a previous study [15], the heat generated in a medium due to ultrasound, q , and the root-mean-square (RMS) sound pressure, p , have the following relationship:

$$q = 2\alpha \frac{p^2}{\rho_0 c_0}, \quad (1)$$

where α , ρ_0 , and c_0 denote the attenuation coefficient, medium density, and speed of sound, respectively. Thus, using q , the heat conduction equation of the medium is as follows:

$$\rho_0 C \frac{\partial T}{\partial t} = \nabla \cdot (k \nabla T) + q, \quad (2)$$

where C , k , and T denote the specific heat, thermal conductivity, and air temperature, respectively.

By ignoring the first term on the right-hand side, as the thermal conductivity k of air is small, and the temperature gradient ∇T is small in very short-time ultrasound irradiation, Eq. (2) can be transformed as follows:

$$\rho_0 C \frac{\partial T}{\partial t} = 2\alpha \frac{p^2}{\rho_0 c_0}. \quad (3)$$

Considering that the temperature on the nylon mesh surface inserted in the ultrasound fields, T_n , and the temperature of the air medium, T , are the same by ignoring the heat

capacity of the nylon mesh, Eq. (3) becomes

$$p = \sqrt{\frac{\rho_0^2 c_0 C}{2\alpha}} \sqrt{\frac{\partial T_n}{\partial t}}. \quad (4)$$

As described above, the sound pressure can be estimated from the rate of change of temperature of the nylon mesh surface inserted into the airborne ultrasound fields.

III. QUANTITATIVE EVALUATION OF PROPOSED METHOD

A. Procedure

This section considers the quantitative relationship between the sound pressure and temperature increase rate on the surface of the nylon mesh. As shown in Fig. 1,

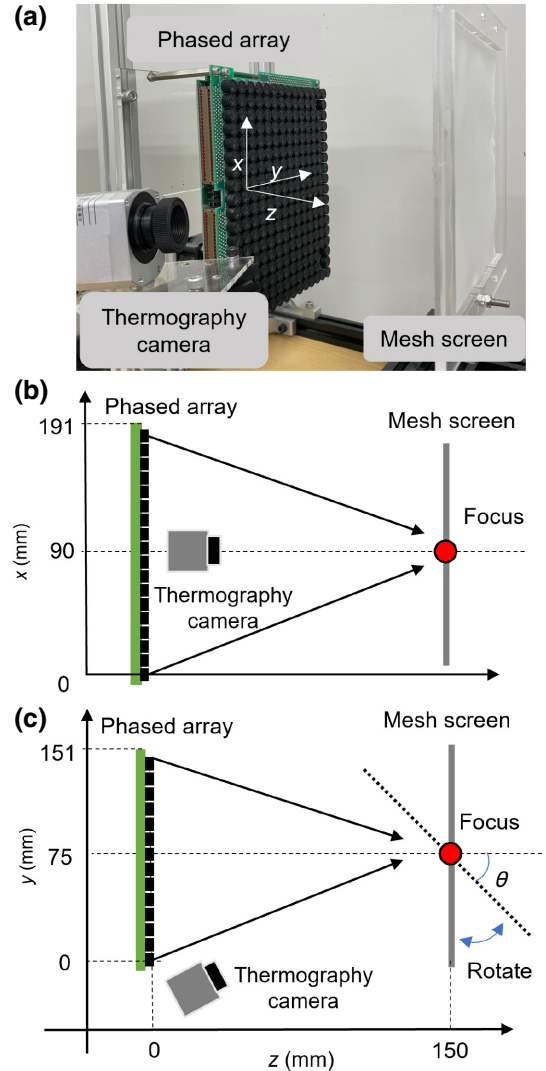


FIG. 1. Experimental setup. (a) Setup image. (b) Setup illustration viewed from the side. (c) Setup illustration viewed from above. The mesh screen is rotated at $\theta = 0^\circ, 30^\circ, 60^\circ$, and 90° .

the experimental setup used in this study consists of a thermography camera, an ultrasound phased array, and a mesh screen. We use a thermography camera (OPTPI 45ILTO29T090, Optris) with an optical resolution of 382×288 px², temperature resolution of 40 mK, and frame rate of 27 Hz. To generate an acoustic field with a single focus, we use an airborne ultrasound phased array consisting of 249 ultrasound transducers (T4010A1, Nippon Ceramic Co. Ltd.) operating at a frequency of 40 kHz, as well as the software architecture developed by Suzuki *et al.* [16]. In addition, we employ a nylon 6.6 mesh (PA-77 μ , AS ONE). We measure the temperature change rate at the location of the focus in the mesh surface at $\theta = 0^\circ, 30^\circ, 60^\circ$, and 90° , as well as the sound pressure at the focus using a standard microphone (type 4138-A-015, Brüel & Kjær). During the experiment, the room temperature and humidity are 26.3 °C and 26.6%, respectively.

B. Results and discussion

Figure 2(a) shows the temperature distribution near the focal point 65 ms before ultrasound irradiation and 431 ms after irradiation of 30% of maximum output amplitude at $\theta = 90^\circ$. Here, the + mark represents the focal point. The time series of the mesh surface temperature are plotted in Figs. 2(b) and 2(c).

Figure 2(c) confirms that the temperature at the focus increases linearly while ultrasound is irradiated for 500 ms from Fig. 2(c). The gradients obtained by fitting using the least-squares method, that is, the rate of temperature change, $\partial T/\partial t$, are 1.11, 0.70, 0.59, and 0.49 K/s at $\theta = 0^\circ, 30^\circ, 60^\circ$, and 90° , respectively.

According to a previous study [9], the attenuation coefficient α is 1.15×10^{-1} Np/m. Considering that ρ is 1.18 kg/m³, c_0 is 347 m/s, and C is 1006 J/kg K when the air temperature is 26.3 °C, a p value of 1.01 kPa can be obtained from $\partial T/\partial t = 0.49$ K/s at $\theta = 0^\circ$ by using Eq. (4). The theoretical predictions agreed well with the microphone measurement of 1.15 kPa.

Meanwhile, when the mesh is perpendicular to the ultrasound beam ($\theta = 90^\circ$), the temperature change rate is 1.11 K/s, which is larger than that in the $\theta = 0^\circ$ case. The difference is considered to be due to viscous heat generation around the mesh where the air passes through the narrow mesh apertures. Thus, the heat generation depends on the mesh angle.

The measurement of weak sound pressure within a short time will be considered in future work. Meanwhile, in the high-intensity airborne ultrasound field using multiple ultrasound phased arrays, the temperature distribution helps visualize the ultrasound field in real time. Figure 3 and Video 1 show two types of ultrasound fields generated using four ultrasound phased arrays. The characteristics of the sound field such as the antinode and nodes of the

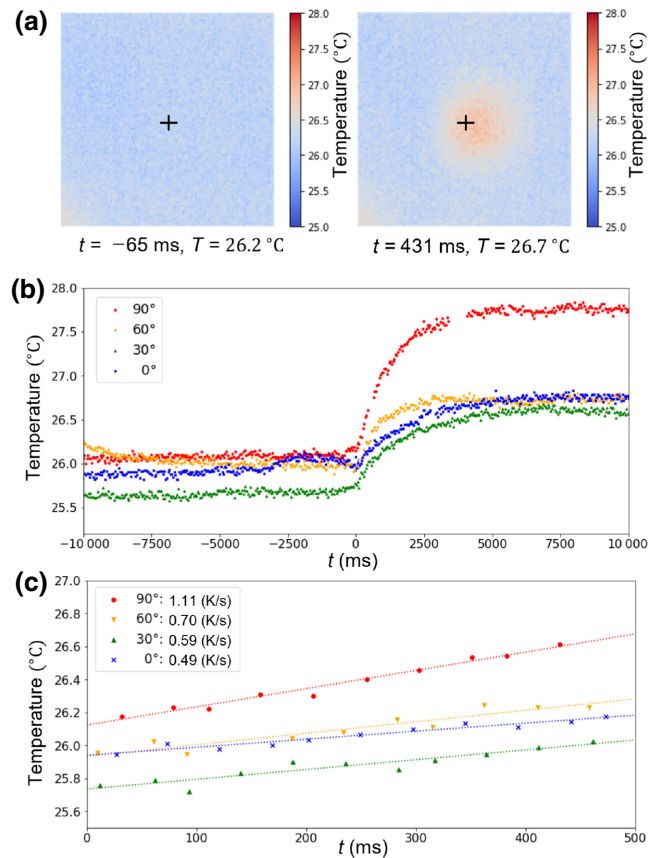


FIG. 2. (a) Temperature distribution at the focal point before ultrasound irradiation ($t = -65$ ms) and after irradiation ($t = 431$ ms). (b) Time series of the temperature at the focal point of the ultrasonic irradiation. The ultrasonic irradiation start time is $t = 0$. (c) Enlarged version of the graph for 0.5 s from the start of irradiation. The gradients of each line correspond to the rate of temperature change, $\partial T/\partial t$, which are 1.11, 0.70, 0.59, and 0.49 K/s at $\theta = 0^\circ, 30^\circ, 60^\circ$, and 90° , respectively.

standing wave and the side lobes of the focal point can be seen.

IV. MEASUREMENT OF TWO-DIMENSIONAL SOUND PRESSURE DISTRIBUTION

A. Procedure

We experimentally confirm that the distribution of the two-dimensional temperature change rate corresponds to the sound pressure distribution. In this experiment, as shown in Fig. 4, the experimental device consists of a thermography camera, two ultrasound phased arrays, and a mesh screen. The surface temperature of the mesh screen when a standing wave is generated using two ultrasound phased arrays facing each other is measured with a thermography camera. Next, the sound pressures at $x = 90$, $y = 81$, and $-120 < z < 180$ in Fig. 4 are scanned with a microphone in 0.1-mm intervals. However, because the microphone used has a limitation that it can only measure

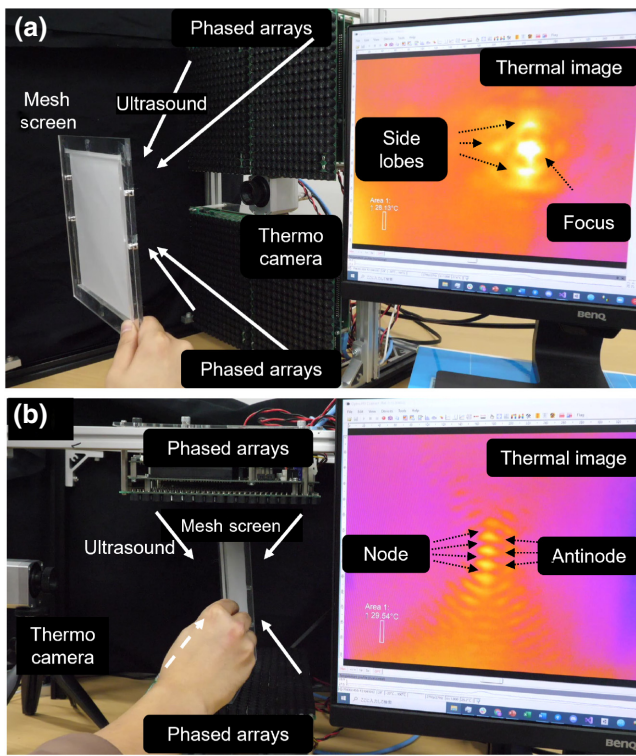
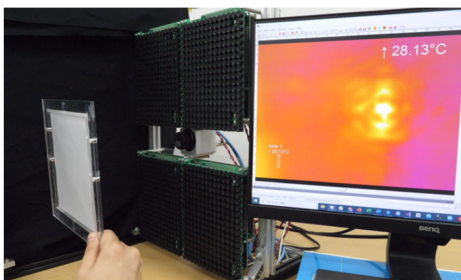


FIG. 3. (a) The image shows a mesh screen, four ultrasound phased arrays, a thermography camera, and one frame of thermal images on the display. First, the ultrasound phased arrays generate an acoustic standing wave. Then, the mesh screen is manually placed inside the acoustic field. We can see that the frame can be used to visualize the features of the standing wave, particularly the nodes and antinodes. (b) Same setup as in (a) except for the position of the infrared camera and the arrangement of the four ultrasound phased arrays, which are modified to generate an acoustic field with a single focus. We can see that the frame reveals the acoustic field, including its focal point and side lobes.

sound pressure up to 5000 Pa, the output amplitude of the phased array is reduced to 3% for accurate measurement of the sound pressure distribution. The room temperature and humidity at the time of the experiment are 21.6 °C and 25.5%, respectively.



VIDEO 1. Visualization of the ultrasound fields in the air using a thermography camera and a mesh screen.

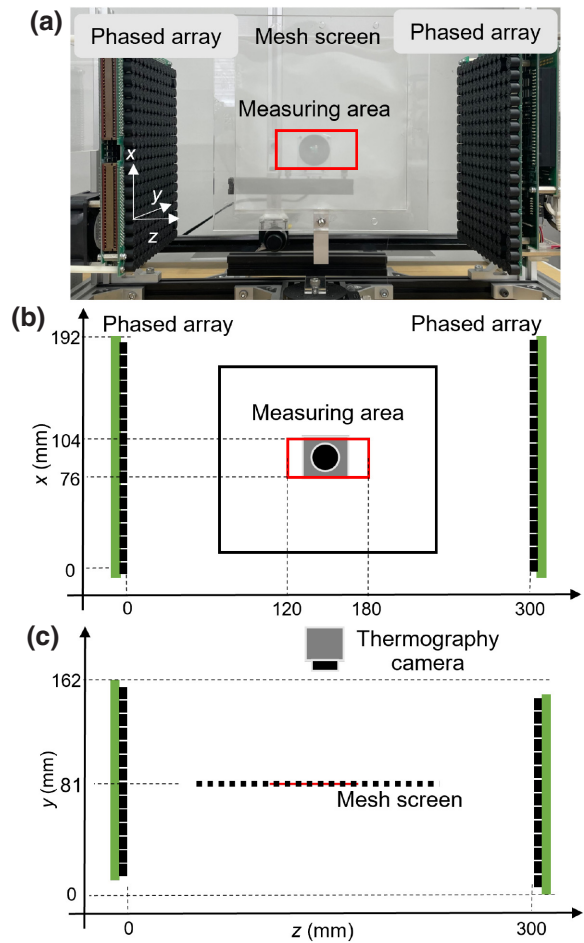


FIG. 4. Experimental setup. (a) Setup image. (b) Setup viewed from the side. (c) Setup viewed from above.

B. Results and discussion

Figure 5(a) depicts the temperature change rate distribution on the surface of the mesh screen inserted into the standing wave for 501 ms from the start of ultrasound irradiation at maximum output. In Fig. 5(b), the position z is plotted on the horizontal axis, and the temperature change rate $\partial T/\partial t$ (K/s) and the sound pressure P (Pa) are plotted on the vertical axis. From this figure, it can be seen that the distribution of the temperature change rate corresponds to the sound pressure distribution.

Another possible factor contributing to the temperature rise on the mesh surface is the viscous heat generated due to the interaction between the mesh and air depending on the particle velocity. However, in the antinode of the sound pressure of the standing wave, a large temperature rise is confirmed even though the particle velocity is theoretically zero. These findings confirm that the major contributor to the temperature rise in this case is the heat generation of the air itself described in Sec. II.

The fact that the sound pressure can be estimated from the temperature rise of the medium itself can also be

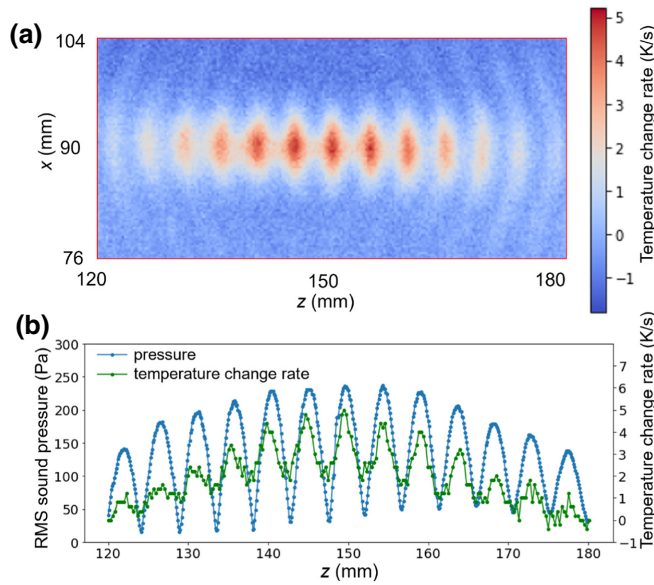


FIG. 5. (a) Temperature distribution on a mesh placed within a standing wave. x and z represent spatial positions. (b) Temperature change rate and the RMS of the sound pressure versus z position. This figure demonstrates that the temperature increases significantly at the antinode of the standing wave, where the sound pressure is high.

applied to the measurement of the ultrasound field on the surface of an object that completely reflects ultrasound. A temperature increase is observed even on the surface of a 3-mm-thick acrylic plate (Fig. 6). The experimental setup is the same as in Fig. 1, with the acrylic plate placed at the

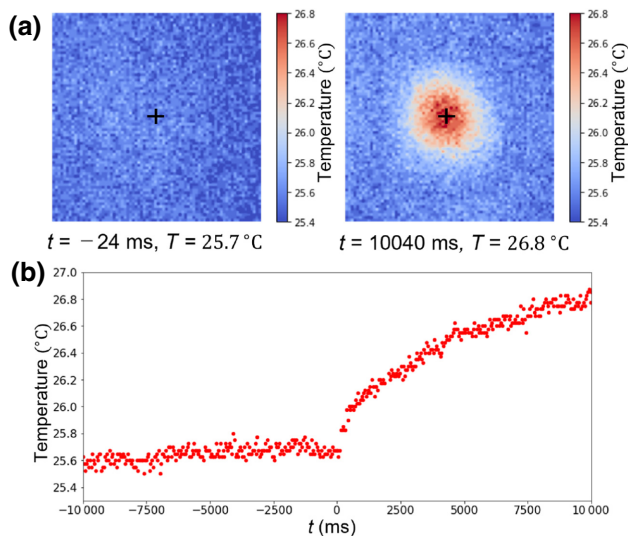


FIG. 6. (a) Temperature distribution at the focal point on the acrylic plate before ultrasound irradiation ($t = -24$ ms) and after irradiation ($t = 10\ 040$ ms). (b) Time series of the temperature at the focal point of the ultrasound field. The ultrasonic irradiation start time is $t = 0$.

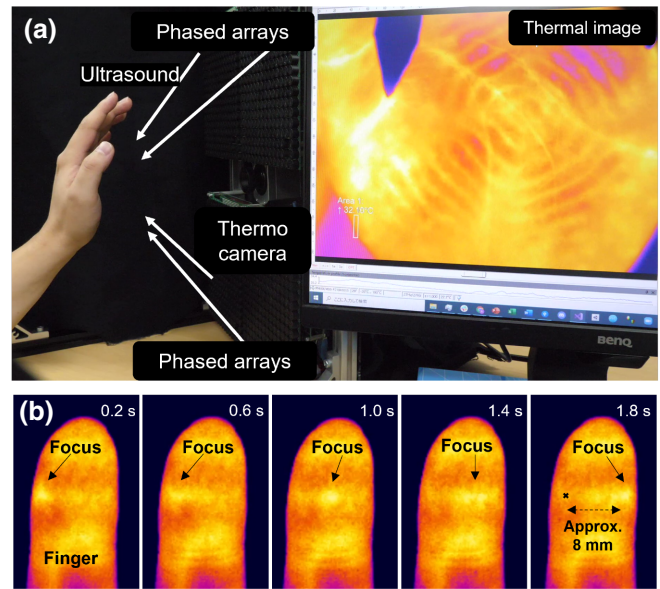
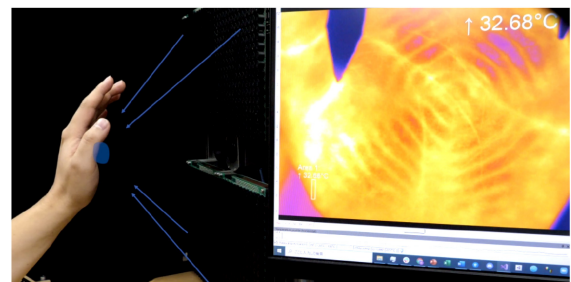


FIG. 7. (a) Photography of a hand, four ultrasound phased arrays, a thermography camera, and one frame of thermal images. First, the ultrasound phased arrays generate an acoustic field with a single focus. Then, a left hand is placed in front of the acoustic field. The frame describes the thermal distribution on the hand. A concentric circle pattern that visualizes the acoustic field is visible on the palm. (b) Image sequence showing the thermal distribution on the fingertip obtained using the same environment as that in (a). The focus is moved in steps of 2 mm every 0.4 s (0.2-s irradiation and 0.2-s stop). It is confirmed that the focus moves in 2-mm steps, resulting in a movement of 8 mm.

position of the mesh screen. The ultrasound field on the surface of the hand, which is the most important for the application to midair haptics, is also visualized. Figure 7 and Video 2 show the thermal images acquired during the experiment.

The distribution of the acoustic field on the palm of the hand and the focal point moving across the fingertip can be observed with a resolution of less than the 8.5-mm wavelength of the emitted 40-kHz ultrasound.

These results indicate that the proposed method is different from the conventional method of measuring sound



VIDEO 2. Visualization of the ultrasound fields on the object's surface using a thermography camera.

pressure by placing an absorbing object in water or *in vivo* and absorbing ultrasound waves to generate heat.

V. CONCLUSION

This paper proposes a method of visualizing the two-dimensional sound pressure distribution in an airborne ultrasound field at high speed using the temperature change rate of air. It is confirmed that the sound pressure estimated from the temperature change rate is almost the same as that measured by a microphone, and that quantitative measurement is possible. It is experimentally confirmed that a two-dimensional sound pressure distribution can be visualized in 0.5 s by using a thermography camera and a nylon mesh. Based on the observation of the temperature rise in the antinode of the sound pressure of the standing wave, it is confirmed that this phenomenon is caused by heat transfer from ambient air heated by ultrasound waves to the mesh. Furthermore, based on the discovery of this phenomenon, it is suggested that the pattern of an airborne ultrasound field on the surface of a hand, which reflects ultrasound waves almost completely, can be observed. In addition, when the focal position is on the fingertip, it is possible to specify it with a resolution finer than the wavelength. We believe that the proposed method of high-speed measurement of airborne ultrasound fields will dramatically advance research on the use of high-intensity airborne ultrasound waves, including airborne tactile sensation and acoustic levitation technologies.

ACKNOWLEDGMENTS

This work is supported in part by JST CREST JPMJCR18A2 and JSPS KAKENHI Grant No. JP20K19841. We would like to thank Editage (www.editage.com) for English language editing.

-
- [1] A. Ozcelik, J. Rufo, F. Guo, Y. Gu, P. Li, J. Lata, and T. J. Huang, Acoustic tweezers for the life sciences, *Nat. Methods* **15**, 1021 (2018).
 [2] A. Marzo, S. A. Seah, B. W. Drinkwater, D. R. Sahoo, B. Long, and S. Subramanian, Holographic acoustic elements

- for manipulation of levitated objects, *Nat. Commun.* **6**, 8661 (2015).
 [3] M. A. Andrade, A. Marzo, and J. C. Adamowski, Acoustic levitation in mid-air: Recent advances, challenges, and future perspectives, *Appl. Phys. Lett.* **116**, 250501 (2020).
 [4] I. Rakkolainen, E. Freeman, A. Sand, R. Raisamo, and S. Brewster, A survey of mid-air ultrasound haptics and its applications, *IEEE Trans. Haptics* **14**, 2 (2020).
 [5] R. Hirayama, D. M. Plasencia, N. Masuda, and S. Subramanian, A volumetric display for visual, tactile and audio presentation using acoustic trapping, *Nature* **575**, 320 (2019).
 [6] K. Hasegawa, H. Yuki, and H. Shinoda, Curved acceleration path of ultrasound-driven air flow, *J. Appl. Phys.* **125**, 054902 (2019).
 [7] V. Contreras and A. Marzo, Adjusting single-axis acoustic levitators in real time using rainbow schlieren deflectometry, *Rev. Sci. Instrum.* **92**, 015107 (2021).
 [8] Z. Xu, H. Chen, X. Yan, M.-L. Qian, and Q. Cheng, Three-dimensional reconstruction of nonplanar ultrasound fields using radon transform and the schlieren imaging method, *J. Acoust. Soc. Am.* **142**, EL82 (2017).
 [9] T. Hoshi, M. Takahashi, T. Iwamoto, and H. Shinoda, Noncontact tactile display based on radiation pressure of airborne ultrasound, *IEEE Trans. Haptics* **3**, 155 (2010).
 [10] B. D. Cook and R. E. Werchan, Mapping ultrasonic fields with cholesteric liquid crystals, *Ultrasonics* **9**, 101 (1971).
 [11] D. Giridhar, R. A. Robinson, Y. Liu, J. Sliwa, V. Zderic, and M. R. Myers, Quantitative estimation of ultrasound beam intensities using infrared thermography: Experimental validation, *J. Acoust. Soc. Am.* **131**, 4283 (2012).
 [12] M. R. Myers and D. Giridhar, Theoretical framework for quantitatively estimating ultrasound beam intensities using infrared thermography, *J. Acoust. Soc. Am.* **129**, 4073 (2011).
 [13] K. Melde, T. Qiu, and P. Fischer, Fast spatial scanning of 3D ultrasound fields via thermography, *Appl. Phys. Lett.* **113**, 133503 (2018).
 [14] L. Cox, K. Melde, A. Croxford, P. Fischer, and B. W. Drinkwater, Acoustic Hologram Enhanced Phased Arrays for Ultrasonic Particle Manipulation, *Phys. Rev. Appl.* **12**, 064055 (2019).
 [15] T. Cavicchi and W. O'Brien Jr, Heat generated by ultrasound in an absorbing medium, *J. Acoust. Soc. Am.* **76**, 1244 (1984).
 [16] S. Suzuki, S. Inoue, M. Fujiwara, Y. Makino, and H. Shinoda, AUTD3: Scalable airborne ultrasound tactile display, *IEEE Trans. Haptics* **14**, 740 (2021).